Biomedicine & Pharmacotherapy 166 (2023) 115298

Contents lists available at ScienceDirect

Biomedicine & Pharmacotherapy

journal homepage: www.elsevier.com/locate/biopha

# Neuroprotective role of plumbagin on eye damage induced by high-sucrose diet in adult fruit fly *Drosophila melanogaster*

Elisabetta Catalani [a], Simona Del Quondam [a], Kashi Brunetti [a], Agnese Cherubini [a], Silvia Bongiorni [b], Anna Rita Taddei [c], Silvia Zecchini [d], Matteo Giovarelli [d], Clara De Palma [e], Cristiana Perrotta [d], Emilio Clementi [d,f], Giorgio Prantera [b], Davide Cervia [a,*]

[a] Department for Innovation in Biological, Agro-food and Forest systems (DIBAF), Università degli Studi della Tuscia, largo dell'Università snc, 01100 Viterbo, Italy
[b] Department of Ecological and Biological Sciences (DEB), Università degli Studi della Tuscia, largo dell'Università snc, 01100 Viterbo, Italy
[c] Section of Electron Microscopy, Great Equipment Center, Università degli Studi della Tuscia, largo dell'Università snc, 01100 Viterbo, Italy
[d] Department of Biomedical and Clinical Sciences (DIBIC), Università degli Studi di Milano, via G.B. Grassi 74, 20157 Milano, Italy
[e] Department of Medical Biotechnology and Translational Medicine (BioMeTra), Università degli Studi di Milano, via L. Vanvitelli 32, 20129 Milano, Italy
[f] Scientific Institute IRCCS "Eugenio Medea", via Don Luigi Monza 20, 23842 Bosisio Parini, Italy

ARTICLE INFO

*Keywords:*
Retina neurodegeneration
*Drosophila melanogaster*
Hyperglycemia
Plumbagin
Redox homeostasis
Autophagy/apoptosis

ABSTRACT

The natural compound plumbagin has a wide range of pharmacological and potential therapeutic activities, although its role in neuroretina degeneration is unknown. Here we evaluated the effects of plumbagin on retina homeostasis of the fruit fly *Drosophila melanogaster* fed with high glucose diet, a model of hyperglycemia-induced eye impairment to study the pathophysiology of diabetic retinopathy at the early stages. To this aim, the visual system of flies orally administered with plumbagin has been analyzed at structural, functional, and molecular/cellular level as for instance neuronal apoptosis/autophagy dysregulation and oxidative stress-related signals. Our results demonstrated that plumbagin ameliorates the visual performance of hyperglycemic flies. Drosophila eye-structure, clearly altered by hyperglycemia, i.e. defects of the pattern of ommatidia, irregular rhabdomeres, vacuoles, damaged mitochondria, and abnormal phototransduction units were rescued, at least in part, by plumbagin. In addition, it reactivated autophagy, decreased the presence of cell death/apoptotic features, and exerted antioxidant effects in the retina. In terms of mechanisms favoring death/survival ratio, Nrf2 signaling activation may be one of the strategies by which plumbagin reduced redox unbalance mainly increasing the levels of glutathione-S-transferase. Likewise, plumbagin may act additively and/or synergistically inhibiting the mitochondrial-endoplasmic reticulum stress and unfolded protein response pathways, which prevented neuronal impairment and eye damage induced by reactive oxygen species. These results provide an avenue for further studies, which may be helpful to develop novel therapeutic candidates and drug targets against eye neurotoxicity by high glucose, a key aspect in retinal complications of diabetes.

## 1. Introduction

Retinal disorders are becoming more prevalent and numerous globally over time, also supported by the increment in life expectancy. Among different types of retinopathies, glaucoma, age-related macular degeneration, and diabetic retinopathy (DR) may share symptoms and treatments. Concerning DR, hyperglycemia is the main metabolic factor associated with its onset and progression. All retinal cells are involved in the pathophysiology of DR that includes microvascular complications, breakdown of the blood-retinal barrier (BRB), inflammation, oxidative stress, and neurodegeneration as typical hallmarks [1,2]. Of notice, retinal neurons may be altered by hyperglycemia before the occurrence of clinical DR symptoms since early damages in the neuroretina can promote vascular abnormalities [3–5]. Clinical medications or surgeries approved to treat DR (also off label) [6] include the intravitreal delivery of anti-vascular endothelial growth factor agents that may stop growth of new blood vessels and decrease fluid buildup, thus reducing DR progression and/or increasing the likelihood of DR regression. Ocular injections of corticosteroids help to decrease prompt fluid reabsorption and cellular swelling, thus reducing vascular permeability and restoring

* Corresponding author.
*E-mail address:* d.cervia@unitus.it (D. Cervia).

https://doi.org/10.1016/j.biopha.2023.115298
Received 23 June 2023; Received in revised form 3 August 2023; Accepted 5 August 2023
Available online 17 August 2023

BRB integrity. The leakage of blood and fluid in the eye may be also slowed down by focal laser treatment while scatter laser treatment can shrink the abnormal blood vessels and vitrectomy removes blood from the middle of the eye and scar tissue. Overall, these treatments are fundamental to counteract disease symptoms but are not capable to cure the pathology [2,6]. They are used for the late stages of disease progression and so are not life-changing for patients. In addition, a poor visual prognosis is offered for the early stages of DR, since no management is given other than glycemic control. New strategies acting on retinal neurons early at the molecular or cellular level represent important medical need to prevent DR development. In this respect, natural bioactive compounds could offer a new line of defense against hyperglycemia-induced neurodegeneration, with the efficacy of different formulations and administration in the food as a key aspect to be considered [7].

Many naturally occurring molecules such as flavonoids, phenols, and quinones have biological properties in vivo, including the modulation of free radicals and other damaging products. Among them, 1,4-naphthoquinones and its natural derivatives have been extensively investigated [8]. The plant-based secondary metabolite plumbagin, 5-hydroxy-2-methyl-1, 4-naphthoquinone, is an analog of vitamin K3 originally extracted from Plumbago zeylanica L. and mainly found in root, leaf, and stem bark of different plant families, i.e. Plumbaginaceae, Ebenceae, and Droseraceae [9]. This natural compound has a wide range of pharmacological and potential therapeutic activities including antifungal, antibacterial, antitumor, anti-inflammatory, and neuroprotective effects [8,10–13]. In particular, plumbagin has been studied for its neuronal actions in vitro [14–17] as well as in rodent models of Parkinson's and Alzheimer's Disease [18,19], depression/memory deficits [20], cerebral ischemia [21], focal ischemia stroke [17], neuropathic pain [22], and neurotoxicity [23]. Recent data reported the inhibitory effects of plumbagin in retinal pigment epithelial cells [24,25], although its role in neuroretina degeneration is unknown.

To complement more traditional vertebrate systems, the fruit fly *Drosophila melanogaster* is a very potent in vivo tool for human neurodegeneration, also involving eye diseases [26–28]. The use of Drosophila for exploring pathophysiological alterations in metabolic disorders has increased in the last decades as well as its potential for drug discovery, including bioactive natural compounds [29–32]. Biological processes are very well conserved and homologs of ca. 75% of human disease-related genes are found in the fruit fly. In addition, in the context of a powerful and well-established genetic framework, Drosophila provides a big plus concerning animal husbandry and the short generation time and lifespan. We recently characterized a model of hyperglycemic neuronal damage in fly eyes to study the pathophysiology of degeneration developed in patients at the early stages of DR [33,34]. Drosophila fed with high glucose diet exhibited lower responsiveness to light because of vision defects and progressive damage of photosensitive units. In addition, the retina internal network displayed typical neurodegenerative features, namely apoptosis, oxidative stress, and dysfunctional autophagy flux. This system represents a significant occasion to test strategies counteracting hyperglycemic insult in the neuroretina avoiding vascular complications and overall metabolic effects, thus complementing more traditional DR vertebrate tools.

We recently found that diet supplementation with the alimentary integrator Lisosan G, a powder of bran and germ of grain, exerted a robust and multifaceted protective effect on fly retina, ameliorating neuronal impairment and redox unbalance after hyperglycemia [34]. This approach prompted us to use plumbagin in *D. melanogaster* to evaluate its beneficial actions on retinal neurodegeneration occurring in DR. In particular, we aim to evaluate the efficient activity of oral delivered plumbagin on glucose-induced retinal damage by analyzing the visual system of *D. melanogaster* at structural, functional (visual performances), and molecular/cellular level (neuronal apoptosis/autophagy dysregulation, and oxidative stress-related signals). Our result demonstrated for the first time the neuroprotective properties of plumbagin in vivo against hyperglycemic eye damage.

## 2. Materials and methods

### 2.1. Reagents

Plumbagin (#M18615) was obtained from Molnova (Ann Arbor, MI, USA). Following manufacturer's protocol, dimethyl sulfoxide (DMSO) was used to prepare stock solutions of 100 mM plumbagin, stored in the dark below −20 °C to ensure its stability. Bovine serum albumin (BSA), normal goat serum and Alexa Fluor secondary antibody (#A11010) were purchased from Life Technologies (Monza, Italy). Fluoroshield Mounting Medium containing 4',6-diamidine-2'-phenylindole dihydrochloride (DAPI) and fluorescent phalloidin (iFluor 555, #ab176756) was obtained from Abcam (Cambridge, United Kingdom). Agar 100 resin/propylene oxide and Agar 100 resin were obtained from Electron Microscopy Sciences (Hatfield, PA, USA). Anti-phospho-Akt (#4054), anti-cleaved caspase 3 (#9664), and anti-activating transcription factor 4 (ATF4; D4B8 #11815) were purchased from Cell Signaling Technology (Danvers, MA, USA) while anti-nitrotyrosine (#A-21285) was obtained from Invitrogen-ThermoFisher Scientific (Monza, Italy). Anti-Light-Chain 3 (LC3) (#ab128025) and anti-p62/Sequestosome-1 (SQSTM1) (#P0067) were purchased from Merck Sigma-Aldrich (Darmstadt, Germany). The primers pairs (Table 1) were purchased from Bio-Fab Research srl (Roma, Italy). When not indicated all other chemicals were from Merck Sigma-Aldrich.

### 2.2. Fly husbandry and treatments

All experiments were performed with female and male adult *D. melanogaster* (Oregon-R strain from Bloomington Drosophila Stock Center, Indiana University Bloomington, IN, USA) of the same age. Flies were routinely raised in the incubator at 25 °C (mild acidic pH) on a standard corn meal agar food. Fly food was prepared as follows: 25 g of yellow cornmeal, 25 g of brewer's yeast, 2 g of agar, and 27 g of sucrose (9% w/v) were mixed and dissolved by adding warm plain water to a final volume of 300 ml, the hydration source of the flies. The mixture was autoclaved and the broad spectrum fungicide Nipagin (0,75 g) was added at ca. 50 °C. Subsequently, 10 ml of cooling down mixture was dispensed into vials to reach ca. 25 °C. Adult Drosophila (5–6 days old) were then transferred in the vials for 10 days on either the standard diet (STD) or the high-sucrose diet (HSD, 35% w/v), obtained changing sucrose independently while keeping the other components constant. As

**Table 1**
Primer pairs designed for qPCR analysis.

| Gene name | FlyBase ID | Primer sequence* | Amplicon size |
|---|---|---|---|
| sod | FBgn0003462 | F: 5'-ACCGACTCCAAGATTACGCTC-3'<br>R: 5'-CAGTGGCCGACATCGGAATA-3' | 197 bp |
| cat | FBgn0000261 | F: 5'-CTATGGCTCGCACACCTTCA-3'<br>R: 5'-TCGTCCAACTGGGGAACTTG-3' | 194 bp |
| cncc | FBgn0262975 | F: 5'-GAATGACCGCCGATCTCTTGG-3'<br>R: 5'-GGAGCCCATCGAACTGACA-3' | 101 bp |
| dkeap1 | FBgn0038475 | F: 5'-CAAATACGTGTGACCGAGGTAA-3'<br>R: 5'-ACACAGCCGTGTTGCTCAG-3' | 161 bp |
| gstd1 | FBgn0001149 | F: 5'-CGCGCCATCCAGGTGTATTT-3'<br>R: 5'-CTGGTACAGCGTTCCCATGT-3' | 123 bp |
| hsp70 | FBgn0013279 | F: 5'-CGGAGTCTCCATTCAGGTGT-3'<br>R: 5'-GCTGACGTTCAGGATTCCA-3' | 160 bp |
| rpl32 | FBgn0002626 | F: 5'-GACCATCCGCCCAGCATAC-3'<br>R: 5'-CGGCGACGCACTCTGTT-3' | 138 bp |

* F: forward, R: reverse.

previously detailed [33], standard food of flies contained carbohydrates and protein/fat reservoir; supplemental sucrose increased carbohydrate energy at 90% of calories from carbohydrates. Where indicated, flies were reared on diets supplemented with plumbagin. In particular, the stock solution of plumbagin was diluted in water to prepare working solutions. Working solution was then mixed to food into vials at 25 °C to obtain the final concentration of plumbagin, making sure the concentration of DMSO was < 0.1% in order to avoid poisoning effects. Diets were renewed at day 5 to prevent the degradation of the test compound by transferring flies to a new vial containing fresh diet. Of notice, Drosophila food containing high concentrations of brewer's yeast showed considerable buffering capacity [35].

### 2.3. Phototaxis assay

Response to light was assessed as reported before [33,34,36]. Briefly, a plastic vial (2.5 ×9.5 cm) with *D. melanogaster* was inserted and connected to a glass tube (3.0 ×23.0 cm) by transparent tape. The transparent apparatus (30 cm) was placed horizontal and perpendicular to the light source. The directional light source from one side, placed horizontally 15 cm away from the tube, acted as an attractant for the flies. In a dark room 15–20 flies were independently introduced in the apparatus and left separately for 30 min. This allowed adaptation of the flies to darkness. The apparatus was then gently pounded down to place the flies at the opposite end from the light. The light was turned on and a timer was started. A camera was recording fly behavior and their movement (horizontal walking) towards the light source during the experiment (2 min). Each trial was performed three times, at 1 min intervals, and the results were averaged. For the analysis of visual responses, the flies were counted at 10, 20, 30, 40, 50, 60, and 120 s for each marked part of the apparatus, i.e. 0–10 cm (the chamber nearest to origin), 11–20 cm (the chamber next furthest to origin), and 21–30 cm (the chamber furthest to origin). The measurements of navigation strategies of flies towards the light source [33,36] was adapted from previous reports [37].

### 2.4. Climbing assay, body weight and glucose analysis

Geotaxis was assessed using a climbing assay (negative geotaxis reflex in opposition to the Earth's gravity) as previously published with minor modifications [36]. *D. melanogaster* were separated into cohorts (empty vials) consisting of ca. 20 flies. A horizontal line was drawn 15 cm above the bottom of the vial. After a 10 min rest period, the flies were tapped to the bottom of the vials: all flies were forced to start climbing (vertical walking). The number of flies that climbed up to the 15 cm mark after 60 s was recorded as the percentage success rate. A camera was recording fly movement during the experiment. Each trial was performed three times, at 1 min intervals, and the results were averaged.

Flies were also collected in screw cap tubes and weighed in groups of 10 using an ultramicro balance (with high resolution of up to 0.0001 mg). For glucose measurements, whole-body samples were manually homogenized in cold Phosphate Buffer (PB). Supernatants were collected, heated for 10 min at 70 °C, and centrifuged for 3 min at maximum speed (4 °C) before plating. Reagents from glucose assay kit (#GAGO20, Merck Sigma-Aldrich) were then added (37 °C for 40 min) following manufacturer's instructions. The reaction was stopped by adding 12 N $H_2SO_4$ before the measurements of absorbance at 540 nm. The free glucose concentration was determined by comparing the free glucose measurements for each sample to the glucose standard curve [38].

### 2.5. Fluorescence microscopy

*D. melanogaster* heads and bodies were immersion-fixed overnight or for 48 h, respectively, in 4% paraformaldehyde in 0.1 M PB at 4 °C, transferred to 12% sucrose in PB, and stored at 4 °C for at least 24 h. Longitudinal and cross Section (10 μm) were obtained by a cryostat, mounted onto positive charged slides and stored at −20 °C until use. To allow proper comparison in retina, fat body, and muscle analysis, the same depth/region of the structure was sectioned. Fluorescent phalloidin (F-actin staining, 1:2500) was used for observation with: i) LSM 710 confocal microscope (Carl Zeiss, Oberkochen, Germany) (eye cross sections), and ii) Axioskop 2 plus conventional microscope (Carl Zeiss, Oberkochen, Germany) equipped with the Axiocam MRC photo camera and the Axiovision software (eye and muscle longitudinal sections).

For immunostaining detection [39], eye and fat bodies longitudinal sections were washed in PB and then pre-incubated for 30 min at room temperature with 5% BSA and 10% of normal goat serum in PB containing 0.5% Triton X-100. Pre-treated sections were incubated overnight at 4 °C with one of the following rabbit primary antibodies: anti-phospho-Akt (1:25), anti-cleaved caspase 3 (1:500), anti-LC3 (1:100), anti-p62/SQSTM1 (1:200), anti-nitrotyrosine (1:100), and anti-ATF4 (1:100) [40–50] in PB containing 0.5% Triton X-100. Following washes in PB, the sections were incubated in the Alexa Fluor goat anti-rabbit 546 secondary antibody (1:200) in PB overnight at room temperature. When appropriate, the slides were coverslipped with Fluoroshield Mounting Medium containing DAPI for nuclei detection. Incubation in secondary antibodies alone was routinely performed as a negative control. Images were acquired by a Zeiss LSM 710 confocal microscope and the distance between adjacent focal planes (z-stacks) was set at 1 μm. As previously published [33,34,36], the analysis of cleaved caspase 3, LC3, p62, nitrotyrosine, and ATF4 immunostaining was carried out on the single images of each eye section. Each image was converted to grayscale and normalized to background using Adobe Photoshop (Adobe Systems, Mountain View, CA, USA). Mean gray levels were then measured in the selected areas [51].

### 2.6. Transmission Electron Microscopy (TEM)

*D. melanogaster* heads samples were fixed and dehydrated in agreement with previous studies [33,34,36,52]. The dehydration was followed by two steps in pure propylene oxide for 10 min each, at 4 °C. Samples were then infiltrated with mixtures of Agar 100 resin/-propylene oxide in different percentages. At the end of the procedure, samples were embedded in pure Agar 100 resin and let to polymerize for 2 days at 60 °C. Resin blocks were cut with Reichert Ultracut ultramicrotome using a diamond knife. Ultrathin sections (60–80 nm) (Leica Microsystems,Wetzlar, Germany) were collected on copper grids, stained with uranyl acetate and lead citrate, and observed with a JEOL 1200 EXII electron microscope (Jeol, Tokyo, Japan). Micrographs were captured by the Olympus SIS VELETA CCD camera equipped with iTEM software (Olympus, Tokyo, Japan).

### 2.7. Determination of reactive oxygen species (ROS)

As previously published with minor modifications [33,34], ca. 100 head's fly per experimental group were weighted and then homogenized in 10 mM Tris-buffer, pH 7. The homogenates were centrifuged (1000 rpm) for 5 min at 4 °C, and 100 μl of each supernatant were incubated in the presence of 5 μM 2',7'-Dichlorofluorescin diacetate (DCFH-DA) at 37 °C for 60 min. Two-electron oxidation of DCFH results in the formation of the fluorescent product DCF, which was recorded at the end of the incubation at an excitation wavelength of 488 nm and an emission wavelength of 525 nm in a DTX 880 Multimode Detector (Beckman Coulter, Brea, CA, USA).

### 2.8. RNA Extraction and PCR

The analysis of mRNA expression in ca. 25 heads of Drosophila was performed in PureZOL reagent (Bio-Rad, Hercules, CA, USA). Total RNA (500–800 μg) was retro-transcribed using iScript gDNA Clear cDNA Synthesis Kit (Bio-Rad). Quantitative PCR (qPCR) was performed using

SsoAdvanced™ Universal SYBR Green Supermix (Bio-Rad) and the CFX96 Touch Real-Time PCR Detection System (Bio-Rad) [53–56]. The primers pairs are detailed in Table 1. Rpl32 has been used as housekeeping gene for normalization by using the $2^{-\Delta\Delta CT}$ method.

### 2.9. 3-(4,5-dimethylthiazol-2-yl)−2,5-diphenyltetrazolium bromide (MTT) assay

The mitochondrial viability in whole body/head homogenate of Drosophila was performed as previously published with minor modifications [47,57,58]. Briefly, 20 flies and ca. 100 heads were weighed and manually homogenized in cold PB. The supernatants were collected after each consecutive centrifugation at 4 °C, for 5 min, at 1500 and 1000 rpm, respectively. Mitochondrial activity was then evaluated using the MTT reduction method (0.5 mg/ml of final concentration) at absorbance of 595 nm.

### 2.10. Statistics

Generally, sample size calculation was conceptualized with 5% alpha error, 80% power and appropriate effect strength. Samples were only excluded from analyses due to technical problems, e.g. pipetting error, loss/spill of samples, or defects in materials/hardware. F-test was performed to evaluate the homogeneity of variance and Shapiro-Wilk test was used for evaluating data normality. The statistical significance of raw data between the groups (completely randomized) in each experiment was evaluated using unpaired Student's *t*/Mann-Whitney tests (single comparisons) or one-way ANOVA followed by the Tukey post-test (multiple comparisons). A p-value $\leq 0.05$ was considered statistically significant. Data belonging from different experiments were represented and averaged in the same graph. The GraphPad Prism software package (GraphPad Software, San Diego, CA, USA) was used. The results were expressed as means ± SEM of the indicated n values.

## 3. Results

### 3.1. Plumbagin ameliorates visual deficits

A preliminary dose-response, i.e. 1 nM, 10 nM, 30 nM, 100 nM, and 1 μM of plumbagin was tested for 10 days under a controlled sucrose regimen (STD), evaluating general behaviors of flies and their survival rate. At micromolar and submicromolar concentrations plumbagin appeared somewhat toxic at visual observations and significantly decreased the viability of Drosophila while 1–30 nM plumbagin had no effects (Fig. 1A). Therefore, subsequent experiments were performed using plumbagin in food at a final concentration of 30 nM.

The functional investigation of visual system of adult D. *melanogaster* was performed by a phototaxis assay. Accordingly to previous observations [33,34,36], many flies raised under a normal sucrose regimen for 10 days reached the light (furthest chamber from the origin) in a time-dependent manner with a maximum at 60–120 s while less HSD-treated animals were counted in the furthest chamber and reached it more slowly (Fig. 1B). Of interest, the administration of 30 nM plumbagin robustly ameliorated the light response of HSD flies. As shown in Fig. 1C, HSD + plumbagin-treated Drosophila reaching the light at the end of the experiment significantly increased vs HSD to values slightly below STD. The navigation behavior of flies was then evaluated as an index of visual response. A normal behavior consists of flies that move straight towards the light source, while a defective behavior consists of motionless animals and those moving perpendicular to the light or unbiased towards and away from the light. The number of impaired Drosophila was higher in HSD vs STD [33] while the presence of plumbagin was devoid of significative effects (Fig. 1D).

### 3.2. Plumbagin does not affect systemic hyperglycemic status

The impact of plumbagin supplementation on the overall behavioral/metabolic profile of HSD Drosophila at short term was then investigated. The climbing ability (vertical walking) of *D. melanogaster* in our experiments was almost comparable. Indeed, as shown in Fig. 2A, the performance of adult animals raised for 10 days with HSD + plumbagin (30 nM) was not different as compared to HSD and STD in the negative geotaxis assay at 60 s. This scenario was confirmed by fluorescent phalloidin staining to visualize actin striations of somatic muscles of the thorax dorsal lateral segments. Indeed, careful examination of myofiber structure revealed no differences between groups (Fig. 2B).

At the end of the treatments Drosophila were weighed, harvested, and the whole-body glucose quantified. As shown in Fig. 2C-D, plumbagin did not affect the body weight and the high glucose content of HSD flies. In addition, phospho (active)-Akt staining in adipose tissue was evaluated as a reliable indicator of the establishment of insulin resistance [33]. Confocal immunofluorescence revealed that Akt was similarly active and almost completely localized in the nucleus of the fat bodies in both HSD and HSD + plumbagin groups (Fig. 2E).

### 3.3. Plumbagin restores retinal disorganization

Longitudinal and cross sections of the Drosophila eye were labeled with phalloidin to show the array of ommatidia and rhabdomeres, which are the actin-rich apical portion of the photoreceptor containing microvilli and light-sensing proteins [26]. Fluorescence microscopy revealed that 30 nM plumbagin is able to rescue the phenotype of adult animals raised for 10 days with HSD. Indeed, typical hallmarks of hyperglycemic fly retinal neurons such as the abnormal aspect of rhabdomere columns and the disorganization of the hexagonal ommatidia profile [33,34] were not detectable after diet supplemented with plumbagin (Fig. 3A-B).

Similar results were obtained by TEM microscopy in ultrathin longitudinal and cross sections, also showing the higher number of vacuole-like structures within ommatidia in HSD flies when compared with the other groups (Fig. 3C-D). Further, TEM magnifications of longitudinal sections highlighted the widespread presence of damaged mitochondria typical of HSD eye [34] which decreased after plumbagin (Fig. 3E).

### 3.4. Plumbagin acts on apoptosis and autophagy balance of retinal cells

In *D. melanogaster* fed for 10 days under HSD regimen apoptosis and dysfunctional autophagy flux are neurodegenerative features affecting the internal network of the retina [33,34]. Of note, we observed that diet supplemented with plumbagin (30 nM) reduced significantly the cleaved (active) caspase 3 fluorescent aggregates of hyperglycemic eyes (Fig. 3F), indicating an anti-apoptotic effect.

In addition, the autophagosome turnover in the retina neurons was somewhat restored since the immunostaining of LC3 and p62 autophagy proteins was significantly milder in the HSD + plumbagin group when compared to HSD (Fig. 4A-B). As shown by TEM analysis of the lamina, the ultrastructural features of HSD eye, i.e. the high number of accumulated autophagic vesicles with double or multiple-membrane and containing electron-dense material, vacuoles, and damaged mitochondria [33,34] (Fig. 4C) were reduced in HSD flies administered with plumbagin (Fig. 4D).

### 3.5. Plumbagin ameliorates the oxidative damage in retinal cells and modulates oxidative stress responsive factors

Since oxidative stress is closely related to the retina pathogenesis of HSD Drosophila [33,34] the antioxidant effects of plumbagin were then verified. Using the DCFH-DA probe in fly brains, we found that DCF fluorescence induced by 10 days of HSD regimen was significantly

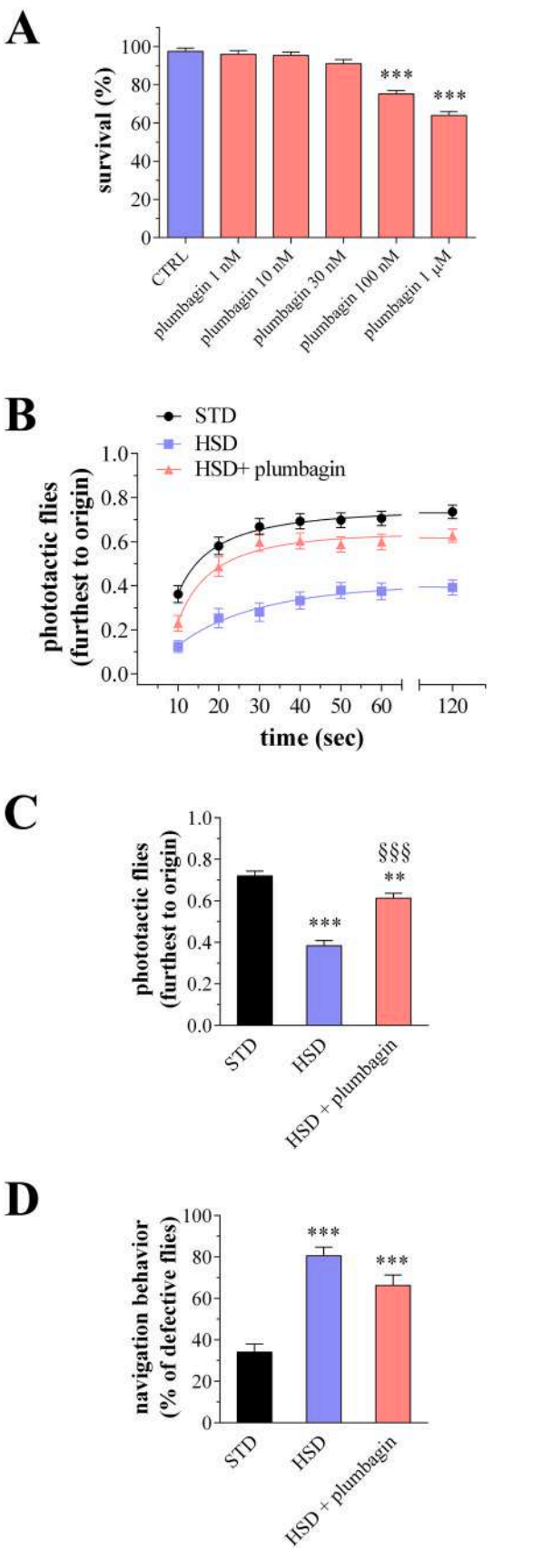


*(caption on next column)*

**Fig. 1.** (A) Survival index of adult *D. melanogaster* growing under STD conditions for 10 days, both in the absence (control, CTRL) and in the presence of increasing concentrations of plumbagin in the food. Results are expressed as the percentage of viable flies at the day 0. *** $p < 0.0001$ vs CTRL. Data are representative of at least $n = 60$ animals obtained from 3 independent experiments. (B-D) Phototaxis assay of adult *D. melanogaster* after 10 days feeding with STD, HSD, and HSD + plumbagin (30 nM). (B) Flies were counted at 10, 20, 30, 40, 50, 60, and 120 s in the chamber furthest to origin (21–30 cm). (C) Flies were analysed in the chamber furthest to origin at 60–120 s. Results are normalized to total flies in the chambers at each time point. (D) Analysis of navigation strategies. Results are expressed as percentage of flies exhibiting a defective behavior within each experimental group. ** $p < 0.001$ and *** $p < 0.0001$ vs STD; §§§ $p < 0.0001$ vs HSD. Data are representative of at least $n = 120$ animals obtained from 7 independent experiments.

decreased by 30 nM plumbagin, indicating lower levels of ROS (Fig. 5A). The inhibition of ROS generation in fly eyes was confirmed by fluorescence immunostaining using an anti-nitrotyrosine antibody to detect peroxynitrite levels. Indeed, retinas under HSD + plumbagin exhibited reduced peroxynitrite labeling when compared with HSD group (Fig. 5B).

In order to investigate the possible modulation of mRNA expression of conserved prototypical oxidative stress response genes, qPCR analysis was performed in extracts of Drosophila heads. As shown in Fig. 5C, transcript levels of superoxide dismutase (SOD) and catalase (CAT) were not affected among experimental groups while HSD administration up-regulated the mRNA levels of glutathione-S-transferase (GstD1) which were further increased by plumbagin. Similar results, i.e. a robust up-regulation after plumbagin, were achieved with cap 'n' collar isoform C (CncC) gene, the homolog of mammalian nuclear factor erythroid 2-related factor 2 (Nrf2). We also found that kelch like ECH associated protein 1 (Keap1) was induced in flies treated with HSD when compared to the control STD. Keap1 regulates Nrf2 transcriptional activity and, of note, plumbagin treatment significantly reduced levels.

In agreement with previous analysis of mitochondrial viability in homogenates of flies hatched from HSD fed larvae [57], we found that adult Drosophila treated for 10 days with HSD displayed impaired mitochondrial activity. Indeed, a decrease of MTT reductive ability was achieved in whole-body when compared with STD condition (Fig. 6A). More important, similar results were found in homogenate of head extracts and, of notice, mitochondrial activity significantly increased in the presence of plumbagin. Organismal responses to mitochondria damage and redox imbalance may involve endoplasmic reticulum (ER) stress and unfolded protein response (UPR) signals [59], which are common between Drosophila and humans [60]. Among them, Drosophila cryptocephal is the homologue of the mammalian ATF4. As shown in Fig. 6B, the immunofluorescence intensity of ATF4 increased in the eye of HSD vs STD flies, while ATF4 staining of hyperglycemic retinas reduced significantly in the presence of plumbagin. Along this line, in heads of HSD Drosophila we found a marked increase of HSP70 mRNA, the major inducible heat shock protein in flies acting as molecular chaperones (Fig. 6C). Diet supplemented with plumbagin was effective in counteracting the overexpressed HSP70.

## 4. Discussion

Plumbagin has gained a lot of attention in research due to its various potential therapeutic actions [8,10–13]. However, there are several challenges such as its limited solubility and oral bioavailability [61]. In Drosophila food passes sequentially through the foregut, anterior midgut, middle midgut, and posterior midgut, and nutrient absorption takes place along this way like in humans [62]. Our feeding experiments in Drosophila were important to demonstrate the activity and delivery of plumbagin in vivo, as a further support towards evaluating its biological effects in the eye. Another limitation of plumbagin is the narrow therapeutic window and the moderate toxicity in animals [61]. Similarly to

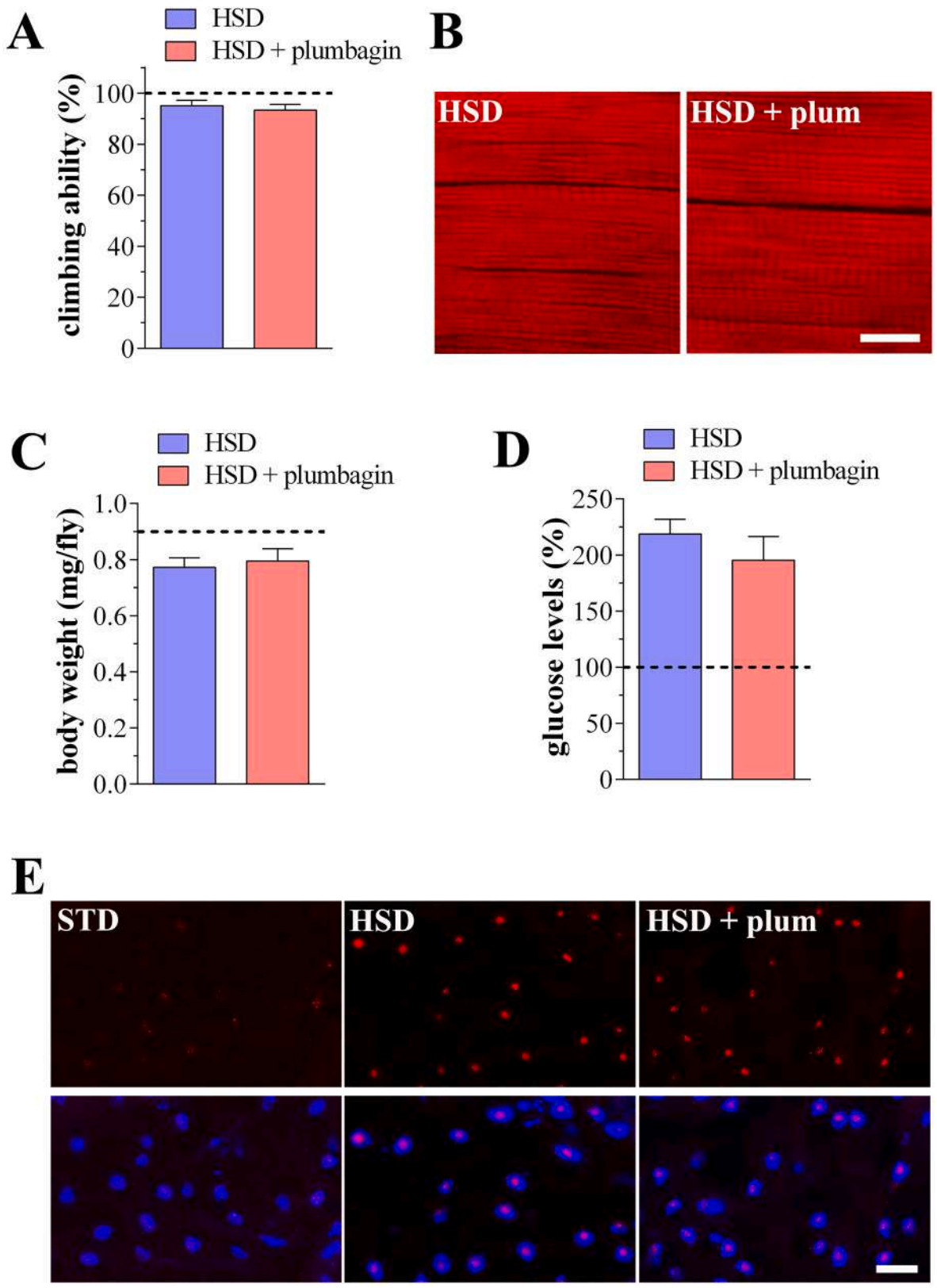


**Fig. 2.** (A) Climbing ability (vertical walking) of adult *D. melanogaster* after 10 days feeding with HSD and HSD + plumbagin (30 nM). Results are expressed as the percentage of flies that climbed up to the 15 cm mark of the vial after 60 s. Dotted line refers to STD group. Data are representative of at least n = 80 animals obtained from 4 independent experiments. (B) Microscopy analysis of longitudinal sections of fly somatic muscles (thorax dorsal lateral segments) stained with the F-actin fluorescent marker phalloidin. Scale bar: 20 μm. Images are representative of at least n = 15 animals obtained from 3 independent experiments. (C) Body weight and (D) whole-body glucose related to the fly weight and expressed as the percentage of STD. Data are representative of at least n = 40 animals obtained from 4 independent experiments. Dotted lines refer to STD group. (E) Confocal microscopy immunofluorescence imaging of phospho-Akt in Drosophila fat bodies. DAPI was used for nuclei detection. Scale bar: 10 μm. Images are representative of at least n = 15 animals obtained from 3 independent experiments.

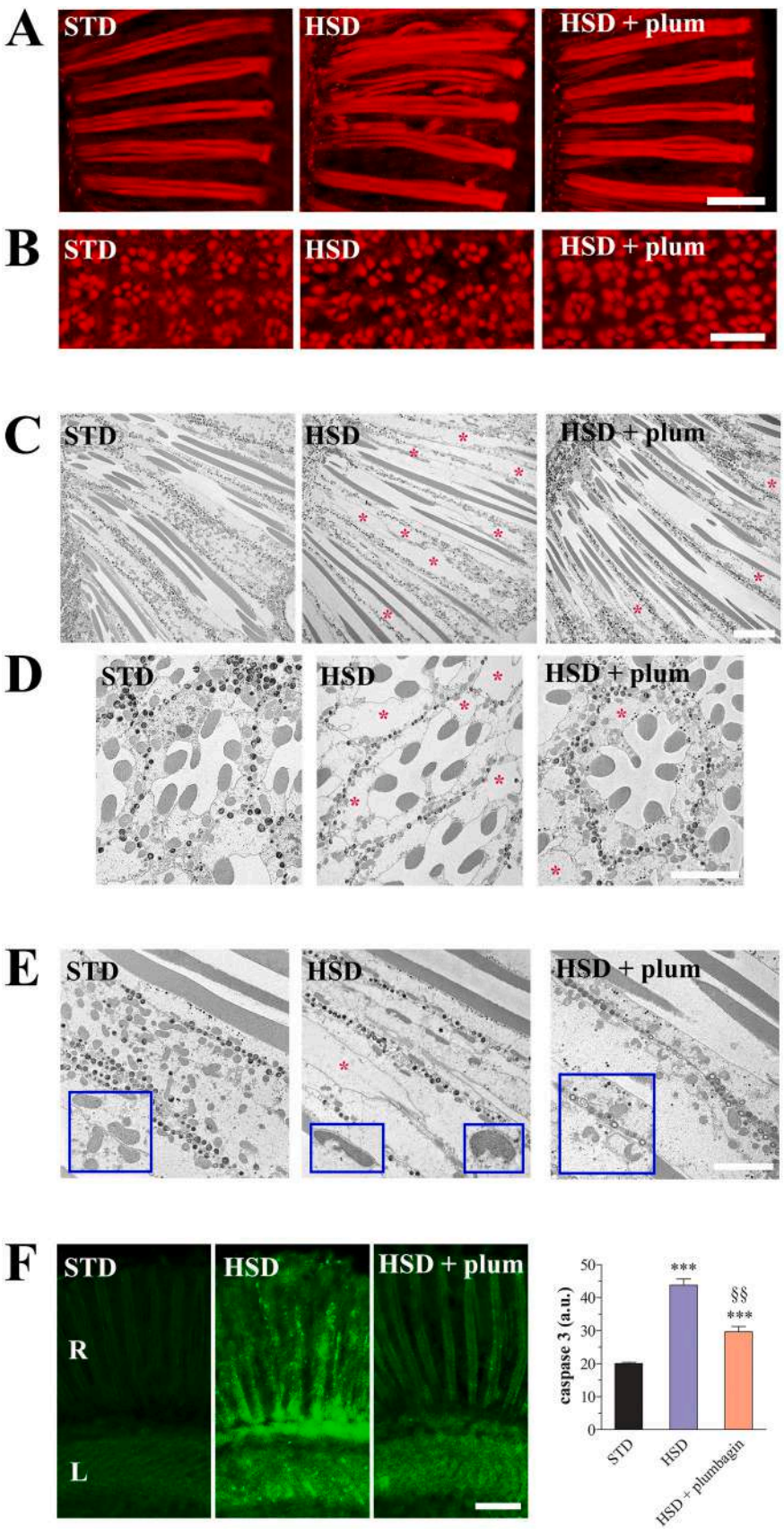


**Fig. 3.** Eye phenotype and apoptosis in adult *D. melanogaster* after 10 days feeding with STD, HSD, and HSD + plumbagin (30 nM). (A) Conventional (longitudinal sections) and (B) confocal (cross sections) microscopy analysis of fly eyes stained with fluorescent phalloidin (F-actin staining) to detect rhabdomere morphology and the pattern of ommatidia and rhabdomeres, respectively. Scale bars: 20 μm (A) and 10 μm (B). Images are representative of at least n = 30 animals obtained from 7 independent experiments. (C-E) Retina ultrastructure by TEM analysis. Longitudinal (C, E) and cross (D) sections of fly eyes. Red asterisks: vacuole-like structures. Inserts (blue boxes) represent enlarged image details of mitochondria. Scale bars: 10 μm (C) and 5 μm (D, E). Images are representative of at least n = 12 animals obtained from 4 independent experiments. (F) Confocal microscopy immunofluorescence imaging of cleaved caspase 3. R: retina, L: lamina. Scale bar: 20 μm. The right graph depicts the quantitative analysis of caspase 3 staining. Results are expressed as arbitrary units (a.u.). *** $p < 0.0001$ vs STD; §§ $p < 0.001$ vs HSD. Images and data are representative of at least n = 30 animals obtained from 7 independent experiments.

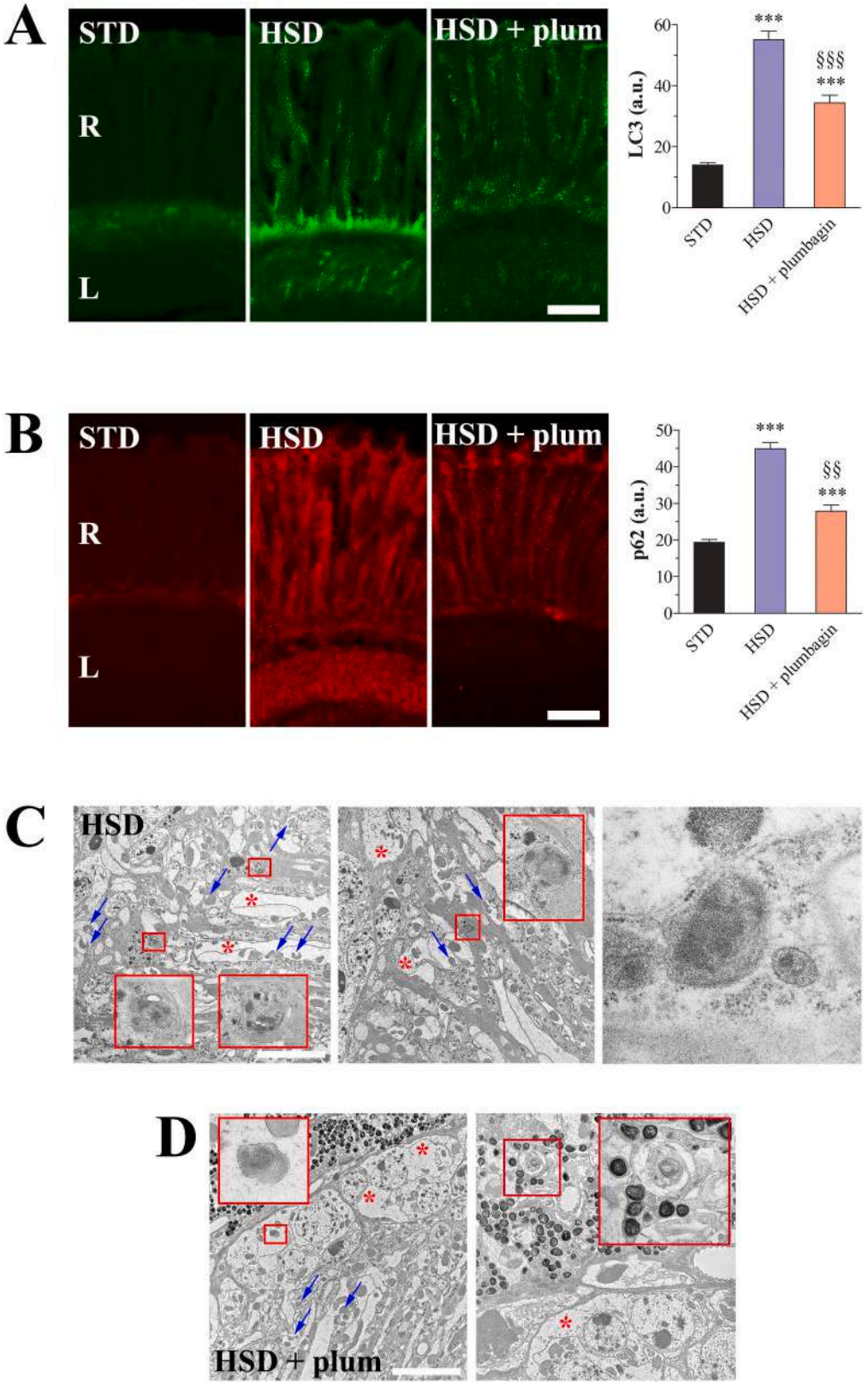


**Fig. 4.** Autophagy in adult *D. melanogaster* after 10 days feeding with STD, HSD, and HSD + plumbagin (30 nM). Confocal microscopy immunofluorescence imaging of (A) LC3 and (B) p62. R: retina, L: lamina. Scale bars: 20 μm. The right graphs depict the quantitative analysis of LC3 and p62 staining. Results are expressed as arbitrary units (a.u.). *** $p < 0.0001$ vs STD; §§ $p < 0.001$ and §§§ $p < 0.0001$ vs HSD. Images and data are representative of at least $n = 30$ animals obtained from 7 independent experiments. (C-D) Eye ultrastructure by TEM analysis showing the presence of accumulated autophagosomes in the lamina and across the lamina-retina. Inserts (red boxes) represent enlarged image details of autophagosomes structures. Red asterisks: vacuoles. Blue arrows: damaged mitochondria. Right panels represent images with increased resolutions. Scale bars: 5 μm. Images are representative of at least $n = 12$ animals obtained from 4 independent experiments.

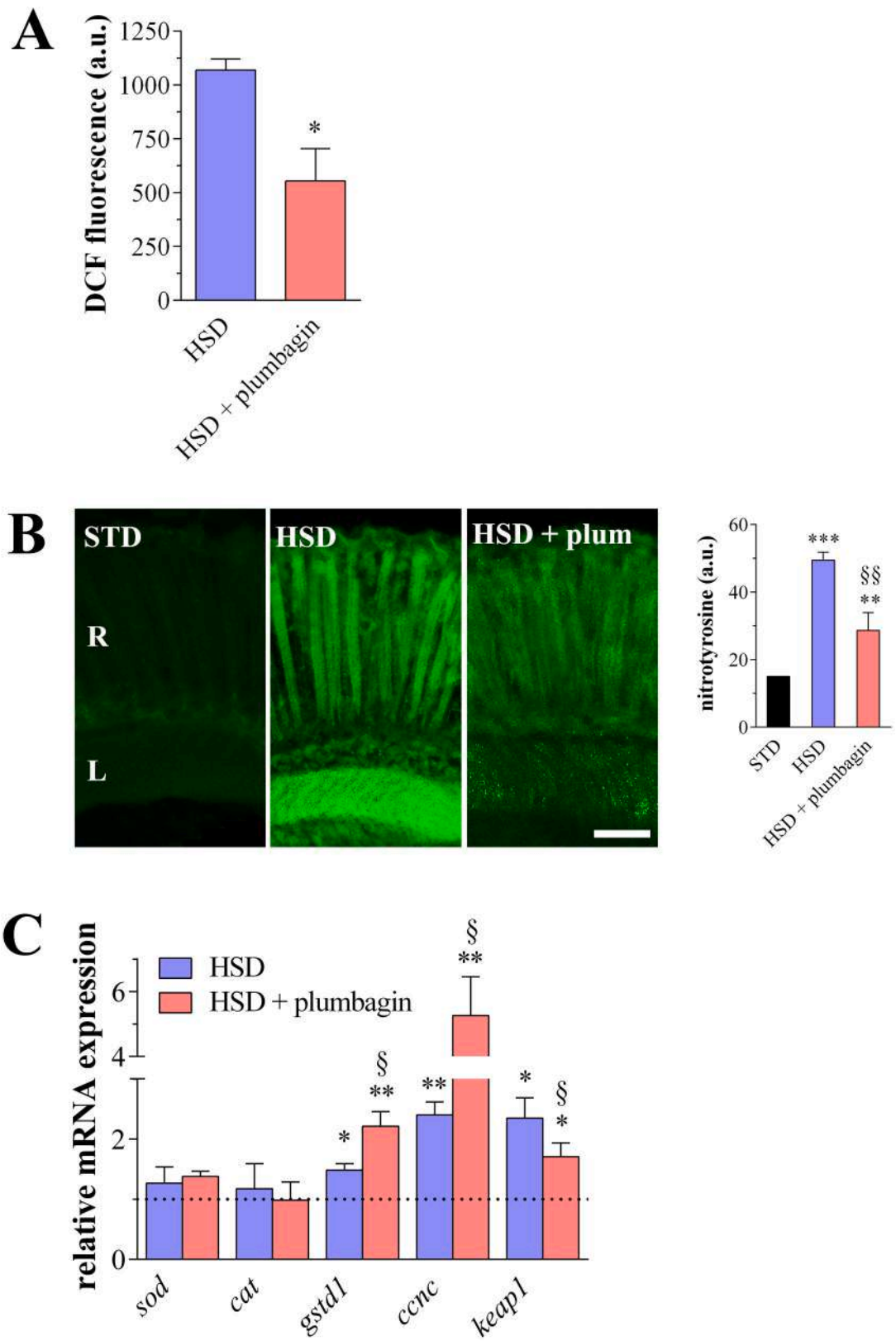


**Fig. 5.** Oxidative stress in adult *D. melanogaster* after 10 days feeding with STD, HSD, and HSD + plumbagin (30 nM). (A) Measurements of ROS by DCF fluorescence intensity in fly heads. Results are expressed as arbitrary units (a.u.). * $p < 0.01$ vs HSD. Data are representative of at least $n = 300$ animals obtained from 3 independent experiments. (B) Confocal microscopy immunofluorescence imaging of nitrotyrosine. R: retina, L: lamina. Scale bar: 20 μm. The right graph depicts the quantitative analysis of nitrotyrosine staining. ** $p < 0.001$ and *** $p < 0.0001$ vs STD; §§ $p < 0.001$ vs HSD. Images and data are representative of at least $n = 30$ animals obtained from 7 independent experiments. (C) mRNA levels of *sod*, *cat*, *gstd1*, *ccnc*, and *keap1* genes by qPCR in fly heads. Results are expressed as fold change of STD (dotted line). * $p < 0.01$, ** $p < 0.001$ and *** $p < 0.0001$ vs STD; § $p < 0.01$ vs HSD Data are representative of at least $n = 100$ animals obtained from 4 independent experiments.

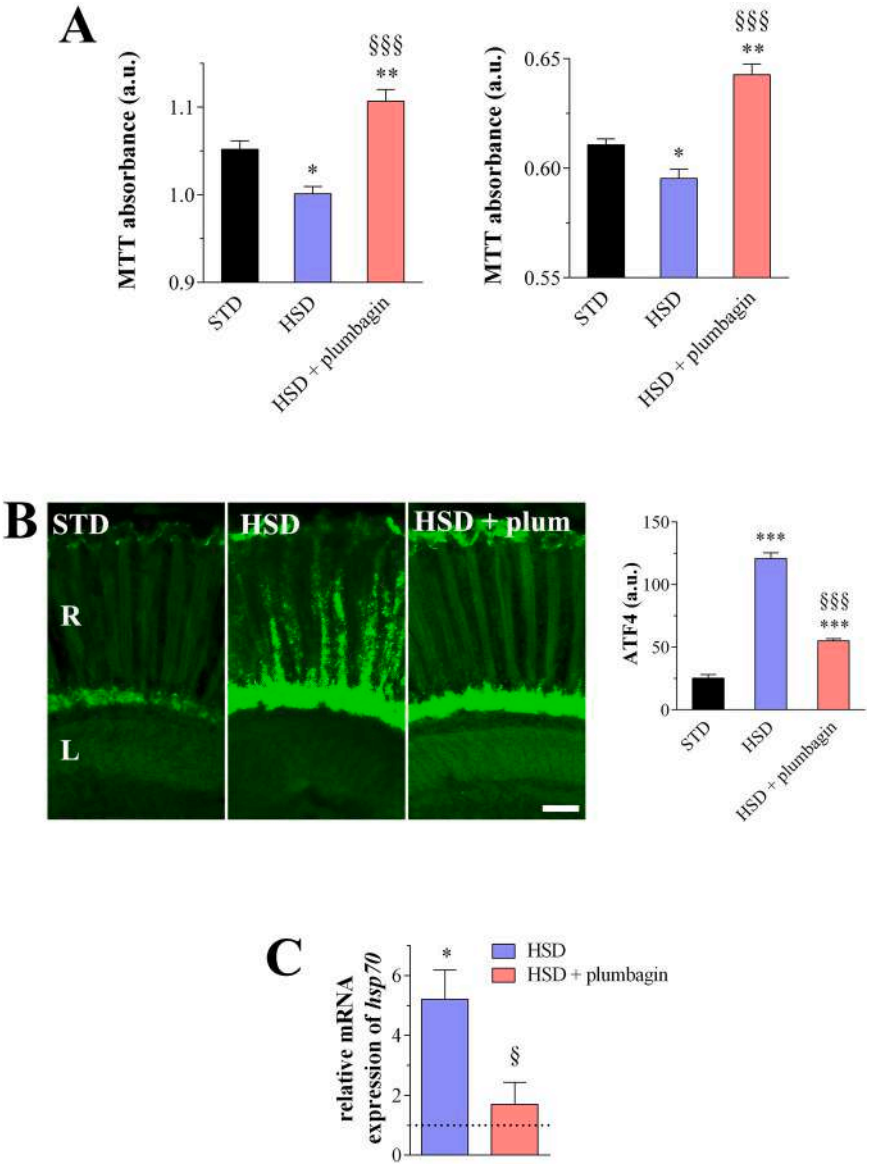


**Fig. 6.** Oxidative stress-related factors in adult *D. melanogaster* after 10 days feeding with STD, HSD, and HSD + plumbagin (30 nM). (A) Measurements of mitochondrial activity by MTT absorbance in whole-body (left panel) and head (right panel) extracts of flies. Results are expressed as arbitrary units (a.u.). * $p < 0.01$ and ** $p < 0.001$ vs STD; §§§ $p < 0.0001$ vs HSD. Data are representative of at least n = 60 (whole-body) and 300 (heads) animals obtained from 3 independent experiments. (B) Confocal microscopy immunofluorescence imaging of ATF4. R: retina, L: lamina. Scale bar: 20 μm. The right graph depicts the quantitative analysis of ATF4 staining. *** $p < 0.0001$ vs STD; §§§ $p < 0.0001$ vs HSD. Images and data are representative of at least n = 30 animals obtained from 7 independent experiments. (C) mRNA levels of *hsp70* gene by qPCR in fly heads. Results are expressed as fold change of STD (dotted line). * $p < 0.01$ vs STD; § $p < 0.01$ vs HSD. Data are representative of at least n = 100 animals obtained from 4 independent experiments.

previous observations in Drosophila [63], preliminary experiments of fly survival allowed to establish 30 nM as the maximum non-toxic dose to be incorporated in orally administered food, in our experimental setting.

At the functional level, the response to light of HSD-treated Drosophila was almost completely restored in the presence of plumbagin, indicating that food supplementation with plumbagin positively affects the vision of flies, which was damaged by hyperglycemia. We also found that the defective navigation behavior of flies persisted over the phototaxis assay thus suggesting that the plumbagin-induced functional recovery was somewhat incomplete. Comparably with ocular injected drugs with beneficial vision effects in rodent models of early DR [64], plumbagin actions were independent of glucose content and body weight. Also, plumbagin did not affect insulin resistance, the health of somatic muscle, and the general locomotor ability/mobility of HSD flies. Similar results on Drosophila were recently achieved with different nutraceutical strategies [34]. This evidence indicates no alterations of major metabolic disturbances and prompted us to hypothesize a direct beneficial role of ingested plumbagin on damaged neuroretina of Drosophila.

We demonstrated that Drosophila eye-structure, clearly altered by hyperglycemic status, i.e. defects of the standard pattern of ommatidia, irregular rhabdomeres, vacuoles, damaged mitochondria, and abnormal phototransduction units were rescued, at least in part, by plumbagin administration. In addition, plumbagin reactivated autophagy and decreased the presence of cell death/apoptotic features in the retina internal network of HSD flies. In visual system damages and ocular health, apoptosis and autophagy have a well-conserved role across species [36,65–69]. In dystrophic Drosophila mutants, we recently found that the impaired autophagy turnover is responsible for retinal apoptosis, structural damage, and vision defects [36]. Of note, the inhibition of cell death by autophagy mechanisms is required for the development of Drosophila eye [70] and retinal degeneration may occur in the presence of defective autophagy [71]. Noteworthy, the autophagy-induced inhibition of apoptosis under DR stress may protect retinal cells in different systems, including Drosophila treated with natural compounds [5,33,34,72–74]. Our data point to the correlation between the positive effects of plumbagin on autophagy/apoptosis balance and the structural/functional recovery of the hyperglycemic fly eye. In other words, the recovery of proper autophagy induced by plumbagin in retina neurons seems to be a key aspect to counteract neurodegenerative/functional features. In this line, plumbagin treatment promoted autophagy and partially repaired the loss of

dopaminergic neurons in Parkinson's disease models [19].

The consumption of HSD in flies triggers oxidative events like in mammals, including ROS accumulation in retina neurons [33,57,75,76]. Comparably with different nutraceutical strategies [34], we demonstrated here that oral administration of plumbagin inhibited brain ROS and retinal peroxynitrite generation in hyperglycemic Drosophila, thus positively affecting their redox steady state, while not altering brain transcripts of SOD and CAT, universal enzymes of organisms that live in the presence of oxygen. We also found that the levels of GstD1, a prototypical oxidative stress response gene encoding well-known detoxification enzymes in flies [77], increased in HSD group, likely as a compensatory response to the elevated ROS levels. Plumbagin further raised GstD1 transcripts, which likely mediate its antioxidant activity. Among regulators of gene expression programs that defend human cells and tissues against oxidative stress, Nrf2 has been extensively characterized [78]. In the absence of oxidative stress, Keap1 complex inhibits Nrf2 transcriptional activity. Upon high glucose–induced oxidative stress, Keap1 is oxidized by upstream activators, for instance ROS, triggering the release of active Nrf2 which induces the expression of redox balancing, detoxifying, stress response, metabolic, and autoregulation factors [79]. The Drosophila CncC is a functional homolog of Nrf2 [80]. Of interest, genetic and cell culture experiments demonstrated that, like its mammalian counterparts, Drosophila Keap1 is a target gene of Nrf2 and acts as an inhibitor of Nrf2, confirming the presence of an auto-regulatory loop in the pathway [80–82]. The activation of the oxidative stress-responsive GstD1 was also reported as a prominent target of CncC/Keap1 system [80,82]. Neurons regulate antioxidant defenses by engaging Nrf2-dependent transcriptional mechanisms and natural products may exert neuroprotective roles by Nrf2 coupling [83,84]. Plumbagin activated Nrf2, increased resistance of cultured neurons to oxidative/metabolic insults, and afforded neuroprotection against ischemic stroke in mouse brain [17]. In addition, β-amyloid-induced neurotoxicity in cultured neurons was inhibited by the antioxidant properties of plumbagin likely through Nrf2 regulation [15]. In a mouse model of retinopathy, a bioactive flavonoid up-regulated the expression of antioxidant enzymes through the Nrf2 pathway and activated autophagy turnover, thus inhibiting retinal oxidative damage [85]. In our system, plumbagin increased the mRNAs of CncC while it inhibited Keap1 levels of HSD flies. Then, Nrf2 (CncC)/Keap1/GstD1 might be key target signaling events for plumbagin-induced protection in Drosophila retina cell and their modulation is associated with the neuronal response to ROS damage during hyperglycemia. Accordingly, the inhibition of Keap1 gene seems to be part of the antioxidant mechanisms, including Gst activation, mediating the protective effects of plant extracts in HSD Drosophila [57]. Noteworthy, Nrf2/Keap1 has been suggested to be a promising target by a number of therapeutics, including phytochemical antioxidants, to counteract hyperglycemia-induced ROS in the onset of different diabetes complications, as for instance diabetic retinopathy [86–88].

The ER stress-UPR is a protein handling network that promotes the elimination of misfolded proteins [59]. It may play an important role in neuronal survival preventing mitochondria damage and ROS generation induced by hyperglycemia [89]. One of the main transcriptional effectors of UPR in nervous system cells is ATF4, an oxidative stress-inducible signal activated by the perturbation of mitochondria that predominantly controls autophagy, protein folding, redox balance, and apoptosis [90–92]. As in other organisms, the stress response was shown to increase Drosophila ATF4 [93–96]. In mouse retinal neurons it has been recently found that genes induced by ATF4 are more relevant to cellular responses against intrinsically generated stressors related to metabolic reprogramming and oxidative stress [97]. We found dysfunctional mitochondria in hyperglycemic Drosophila as well as high levels of ATF4 in retina neurons. Accordingly, there are multiple line of evidence that ATF4 is overexpressed in degenerating retina models, including diabetic retinopathy, and that its downregulation diminished the mitochondrial-ER stress response, preventing cell death and the impairment of vision function [91]. The fact that plumbagin increased mitochondrial activity and reduced ATF4 levels in our system indicates that plumbagin neuroprotective role involves the inhibition of mitochondria-related UPR signals under prolonged ER stress conditions. Redox imbalance and ER stress may trigger recruitment of ER chaperones such as HSP70 family to dysfunctional proteins [98,99]. In Drosophila, the conserved HSP70 was shown to increase during the oxidative damage induced by HSD administration [57]. Our results revealed that plumbagin reduced HSP70 transcript upon hyperglycemia, suggesting the inhibition of stress-induced recruitment of molecular chaperones to restore fly retinal homeostasis.

## 5. Conclusion

Previous results in Drosophila supported the view that hyperglycemia induced by high-sucrose diet leads to eye/neuronal defects and visual dysfunctions which are evolutionarily conserved [33]. Herein, *D. melanogaster* adults were used as a model organism of eye damage triggered by the consumption of sugar-rich diets to test the potential beneficial role of the natural drug plumbagin orally administered. In summary, our results demonstrated that plumbagin ameliorates the visual performance of hyperglycemic flies. Drosophila eye-structure was rescued, at least in part, by plumbagin administration that exerted antioxidant effects on retinal neurons, thus providing efficacious neuroprotection (pro-autophagic and anti-apoptotic actions). In terms of mechanisms favoring death/survival ratio, the Nrf2 signaling activation could be highlighted as one of the strategies by which plumbagin reduced redox unbalance mainly increasing GstD1 levels. Likewise, plumbagin may act additively and/or synergistically inhibiting the mitochondrial-ER stress response and UPR signals, i.e. ATF4 and HSP70, which prevented ROS-induced neuronal impairment and eye damage. These results provide an avenue for further studies, which may be helpful to develop novel therapeutic candidates and drug targets against eye neurotoxicity by high glucose, a key aspect in retinal complications of diabetes.

## Funding

The research has been supported by a grant from the Italian Ministry of University and Research (MUR), PRIN2020 to EClem/DC.

## CRediT authorship contribution statement

**Elisabetta Catalani**: Conceptualization, Investigation, Methodology, Data curation; **Simona Del Quondam**, **Kashi Brunetti**, **Agnese Cherubini**, **Anna Rita Taddei**, **Silvia Zecchini**: Investigation, Methodology, Data curation. **Silvia Bongiorni**, **Giorgio Prantera**: Resources, Validation, Methodology, Supervision, Writing – review & editing. **Matteo Giovarelli**: Formal analysis, Methodology, Visualization. **Clara De Palma**, **Cristiana Perrotta**: Conceptualization, Writing – review & editing. **Emilio Clementi**: Supervision, Funding acquisition, Writing – review & editing. **Davide Cervia**: Conceptualization, Investigation, Supervision, Project administration, Funding acquisition, Writing – original draft, Writing – review & editing.

## Declaration of Competing Interest

None.

## Acknowledgements

We are grateful to the Great Equipment Center (Università degli Studi della Tuscia) for providing access to microscopes and PCR machines.

## References


[1] T.C. Chan, J.L. Wilkinson Berka, D. Deliyanti, D. Hunter, A. Fung, G. Liew, A. White, The role of reactive oxygen species in the pathogenesis and treatment of retinal diseases, Exp. Eye Res. 201 (2020), 108255.

[2] T.Y. Wong, C.M. Cheung, M. Larsen, S. Sharma, R. Simo, Diabetic retinopathy, Nat. Rev. Dis. Prim. 2 (2016) 16012.

[3] R. Simo, C. Hernandez, R. European Consortium for the Early Treatment of Diabetic, Neurodegeneration in the diabetic eye: new insights and therapeutic perspectives, Trends Endocrinol. Metab. 25 (2014) 23–33.

[4] M.G. Rossino, M. Dal Monte, G. Casini, Relationships between neurodegeneration and vascular damage in diabetic retinopathy, Front. Neurosci. 13 (2019) 1172.

[5] E. Catalani, D. Cervia, Diabetic retinopathy: a matter of retinal ganglion cell homeostasis, Neural Regen. Res. 15 (2020) 1253–1254.

[6] S.M. Muns, V.M. Villegas, H.W. Flynn Jr., S.G. Schwartz, Update on current pharmacologic therapies for diabetic retinopathy, Expert Opin. Pharm. (2023) 1–17.

[7] C. Shi, P. Wang, S. Airen, C. Brown, Z. Liu, J.H. Townsend, J. Wang, et al., Nutritional and medical food therapies for diabetic retinopathy, Eye Vis. 7 (2020) 33.

[8] N. Kapoor, P. Kandwal, G. Sharma, L. Gambhir, Redox ticklers and beyond: naphthoquinone repository in the spotlight against inflammation and associated maladies, Pharmacol. Res. 174 (2021), 105968.

[9] A. Roy, N. Bharadvaja, Biotechnological approaches for the production of pharmaceutically important compound: plumbagin, Curr. Pharm. Biotechnol. 19 (2018) 372–381.

[10] S. Padhye, P. Dandawate, M. Yusufi, A. Ahmad, F.H. Sarkar, Perspectives on medicinal properties of plumbagin and its analogs, Med. Res. Rev. 32 (2012) 1131–1158.

[11] A. Roy, Plumbagin: a potential anti-cancer compound, Mini Rev. Med. Chem. 21 (2021) 731–737.

[12] P. Panichayupakaranant, M.I. Ahmad, Plumbagin and its role in chronic diseases, Adv. Exp. Med. Biol. 929 (2016) 229–246.

[13] S. Rajalakshmi, N. Vyawahare, A. Pawar, P. Mahaparale, B. Chellampillai, Current development in novel drug delivery systems of bioactive molecule plumbagin, Artif. Cells Nanomed. Biotechnol. 46 (2018) 209–218.

[14] P. Marrazzo, C. Angeloni, S. Hrelia, Combined treatment with three natural antioxidants enhances neuroprotection in a SH-SY5Y 3D culture model, Antioxidants 8 (2019) 420.

[15] S. Wang, Z. Zhang, S. Zhao, Plumbagin inhibits amyloid-beta-induced neurotoxicity: regulation of oxidative stress and nuclear factor erythroid 2-related factor 2 activation, Neuroreport 29 (2018) 1269–1274.

[16] S.S. Messeha, N.O. Zarmouh, P. Mendonca, M.G. Kolta, K.F.A. Soliman, The attenuating effects of plumbagin on pro-inflammatory cytokine expression in LPS-activated BV-2 microglial cells, J. Neuroimmunol. 313 (2017) 129–137.

[17] T.G. Son, S. Camandola, T.V. Arumugam, R.G. Cutler, R.S. Telljohann, M. R. Mughal, T.A. Moore, et al., Plumbagin, a novel Nrf2/ARE activator, protects against cerebral ischemia, J. Neurochem 112 (2010) 1316–1326.

[18] K.T. Nakhate, A.P. Bharne, V.S. Verma, D.N. Aru, D.M. Kokare, Plumbagin ameliorates memory dysfunction in streptozotocin induced Alzheimer's disease via activation of Nrf2/ARE pathway and inhibition of beta-secretase, Biomed. Pharm. 101 (2018) 379–390.

[19] Y. Su, M. Li, Q. Wang, X. Xu, P. Qin, H. Huang, Y. Zhang, et al., Inhibition of the TLR/NF-kappaB signaling pathway and improvement of autophagy mediates neuroprotective effects of plumbagin in Parkinson's Disease, Oxid. Med. Cell Longev. 2022 (2022) 1837278.

[20] M. Kumar Arora, A. Ratra, S.M.B. Asdaq, A.A. Alshamrani, A.J. Alsalman, M. Kamal, R. Tomar, et al., Plumbagin alleviates intracerebroventricular-quinolinic acid induced depression-like behavior and memory deficits in wistar rats, Molecules 27 (2022) 1834.

[21] X.J. Chen, J.G. Zhang, L. Wu, Plumbagin inhibits neuronal apoptosis, intimal hyperplasia and also suppresses TNF-alpha/NF-kappaB pathway induced inflammation and matrix metalloproteinase-2/9 expression in rat cerebral ischemia, Saudi J. Biol. Sci. 25 (2018) 1033–1039.

[22] V. Arruri, P. Komirishetty, A. Areti, S.K.N. Dungavath, A. Kumar, Nrf2 and NF-kappaB modulation by Plumbagin attenuates functional, behavioural and biochemical deficits in rat model of neuropathic pain, Pharmacol. Rep. 69 (2017) 625–632.

[23] J.H. Yuan, F. Pan, J. Chen, C.E. Chen, D.P. Xie, X.Z. Jiang, S.J. Guo, et al., Neuroprotection by plumbagin involves BDNF-TrkB-PI3K/Akt and ERK1/2/JNK pathways in isoflurane-induced neonatal rats, J. Pharm. Pharmacol. 69 (2017) 896–906.

[24] Y. Zhang, R. Wang, H. Zhang, L. Liu, J. An, J. Hao, J. Ma, Plumbagin inhibits proliferation, migration, and invasion of retinal pigment epithelial cells induced by FGF-2, Tissue Cell 72 (2021), 101547.

[25] H. Chen, H. Wang, J. An, Q. Shang, J. Ma, Inhibitory effects of plumbagin on retinal pigment epithelial cell epithelial-mesenchymal transition in vitro and in vivo, Med. Sci. Monit. 24 (2018) 1502–1510.

[26] E. Catalani, F. Silvestri, D. Cervia, A Drosophila perspective on retina functions and dysfunctions, Neural Regen. Res 17 (2022) 341–343.

[27] P. Gaspar, I. Almudi, M.D.S. Nunes, A.P. McGregor, Human eye conditions: insights from the fly eye, Hum. Genet 138 (2019) 973–991.

[28] H. Bolus, K. Crocker, G. Boekhoff-Falk, S. Chtarbanova, Modeling neurodegenerative disorders in drosophila melanogaster, Int. J. Mol. Sci. 21 (2020) 3055.

[29] M. Xiu, Y. Wang, D. Yang, X. Zhang, Y. Dai, Y. Liu, X. Lin, et al., Using Drosophila melanogaster as a suitable platform for drug discovery from natural products in inflammatory bowel disease, Front. Pharmacol. 13 (2022) 1072715.

[30] S.K. Kim, D.D. Tsao, G.S.B. Suh, I. Miguel-Aliaga, Discovering signaling mechanisms governing metabolism and metabolic diseases with Drosophila, Cell Metab. 33 (2021) 1279–1292.

[31] T.T. Su, Drug screening in Drosophila; why, when, and when not, Wiley Inter. Rev. Dev. Biol. 8 (2019), e346.

[32] U.B. Pandey, C.D. Nichols, Human disease models in Drosophila melanogaster and the role of the fly in therapeutic drug discovery, Pharmacol. Rev. 63 (2011) 411–436.

[33] E. Catalani, F. Silvestri, S. Bongiorni, A.R. Taddei, G. Fanelli, S. Rinalducci, C. De Palma, et al., Retinal damage in a new model of hyperglycemia induced by high-sucrose diets, Pharmacol. Res. 166 (2021), 105488.

[34] E. Catalani, G. Fanelli, F. Silvestri, A. Cherubini, S. Del Quondam, S. Bongiorni, A. R. Taddei, et al., Nutraceutical strategy to counteract eye neurodegeneration and oxidative stress in drosophila melanogaster fed with high-sugar diet, Antioxidants 10 (2021) 1197.

[35] S.A. Deshpande, R. Yamada, C.M. Mak, B. Hunter, A.Soto Obando, S. Hoxha, W. W. Ja, Acidic Food pH Increases palatability and consumption and extends drosophila lifespan, J. Nutr. 145 (2015) 2789–2796.

[36] E. Catalani, S. Bongiorni, A.R. Taddei, M. Mezzetti, F. Silvestri, M. Coazzoli, S. Zecchini, et al., Defects of full-length dystrophin trigger retinal neuron damage and synapse alterations by disrupting functional autophagy, Cell Mol. Life Sci. 78 (2021) 1615–1636.

[37] T.H. Humberg, S.G. Sprecher, Age- and wavelength-dependency of drosophila larval phototaxis and behavioral responses to natural lighting conditions, Front. Behav. Neurosci. 11 (2017) 66.

[38] J.M. Tennessen, W.E. Barry, J. Cox, C.S. Thummel, Methods for studying metabolism in Drosophila, Methods 68 (2014) 105–115.

[39] E. Catalani, F. Buonanno, G. Lupidi, S. Bongiorni, R. Belardi, S. Zecchini, M. Giovarelli, et al., The natural compound climacostol as a prodrug strategy based on pH activation for efficient delivery of cytotoxic small agents, Front. Chem. 7 (2019) 463.

[40] S. Zecchini, F. Proietti Serafini, E. Catalani, M. Giovarelli, M. Coazzoli, I. Di Renzo, C. De Palma, et al., Dysfunctional autophagy induced by the pro-apoptotic natural compound climacostol in tumour cells, Cell Death Dis. 10 (2019) 10.

[41] C. Perrotta, F. Buonanno, S. Zecchini, A. Giavazzi, F. Proietti Serafini, E. Catalani, L. Guerra, et al., Climacostol reduces tumour progression in a mouse model of melanoma via the p53-dependent intrinsic apoptotic programme, Sci. Rep. 6 (2016) 27281.

[42] A. D'Alessandro, D. Cervia, E. Catalani, F. Gevi, L. Zolla, G. Casini, Protective effects of the neuropeptides PACAP, substance P and the somatostatin analogue octreotide in retinal ischemia: a metabolomic analysis, Mol. Biosyst. 10 (2014) 1290–1304.

[43] E. Catalani, F. Proietti Serafini, S. Zecchini, S. Picchietti, A.M. Fausto, E. Marcantoni, F. Buonanno, et al., Natural products from aquatic eukaryotic microorganisms for cancer therapy: Perspectives on anti-tumour properties of ciliate bioactive molecules, Pharm. Res 113 (2016) 409–420.

[44] D. Cervia, M. Garcia-Gil, E. Simonetti, G. Di Giuseppe, G. Guella, P. Bagnoli, F. Dini, Molecular mechanisms of euplotin C-induced apoptosis: involvement of mitochondrial dysfunction, oxidative stress and proteases, Apoptosis 12 (2007) 1349–1363.

[45] D. Cazzato, E. Assi, C. Moscheni, S. Brunelli, C. De Palma, D. Cervia, C. Perrotta, et al., Nitric oxide drives embryonic myogenesis in chicken through the upregulation of myogenic differentiation factors, Exp. Cell Res. 320 (2014) 269–280.

[46] D. Cervia, S. Fiorini, B. Pavan, C. Biondi, P. Bagnoli, Somatostatin (SRIF) modulates distinct signaling pathways in rat pituitary tumor cells; negative coupling of SRIF receptor subtypes 1 and 2 to arachidonic acid release, Naunyn Schmiede Arch. Pharm. 365 (2002) 200–209.

[47] D. Munoz, M. Brucoli, S. Zecchini, A. Sandoval-Hernandez, G. Arboleda, F. Lopez-Vallejo, W. Delgado, et al., XIAP as a target of new small organic natural molecules inducing human cancer cell death, Cancers 11 (2019) 1336.

[48] D. Cervia, C. Petrucci, M.T. Bluet-Pajot, J. Epelbaum, P. Bagnoli, Inhibitory control of growth hormone secretion by somatostatin in rat pituitary GC cells: sst(2) but not sst(1) receptors are coupled to inhibition of single-cell intracellular free calcium concentrations, Neuroendocrinology 76 (2002) 99–110.

[49] D. Cervia, P. Zizzari, B. Pavan, E. Schuepbach, D. Langenegger, D. Hoyer, C. Biondi, et al., Biological activity of somatostatin receptors in GC rat tumour somatotrophs: evidence with sst1-sst5 receptor-selective nonpeptidyl agonists, Neuropharmacology 44 (2003) 672–685.

[50] S. Zecchini, M. Giovarelli, C. Perrotta, F. Morisi, T. Touvier, I. Di Renzo, C. Moscheni, et al., Autophagy controls neonatal myogenesis by regulating the GH-IGF1 system through a NFE2L2- and DDIT3-mediated mechanism, Autophagy 15 (2019) 58–77.

[51] D. Cervia, E. Catalani, M. Dal Monte, G. Casini, Vascular endothelial growth factor in the ischemic retina and its regulation by somatostatin, J. Neurochem. 120 (2012) 818–829.

[52] D. Cervia, E. Assi, C. De Palma, M. Giovarelli, L. Bizzozero, S. Pambianco, I. Di Renzo, et al., Essential role for acid sphingomyelinase-inhibited autophagy in melanoma response to cisplatin, Oncotarget 7 (2016) 24995–25009.

[53] M. Giovarelli, S. Zecchini, G. Catarinella, C. Moscheni, P. Sartori, C. Barbieri, P. Roux-Biejat, et al., Givinostat as metabolic enhancer reverting mitochondrial biogenesis deficit in Duchenne Muscular Dystrophy, Pharmacol. Res. 170 (2021), 105751.

[54] M. Giovarelli, S. Zecchini, E. Martini, M. Garre, S. Barozzi, M. Ripolone, L. Napoli, et al., Drp1 overexpression induces desmin disassembling and drives kinesin-1 activation promoting mitochondrial trafficking in skeletal muscle, Cell Death Differ. 27 (2020) 2383–2401.
[55] L. Bizzozero, D. Cazzato, D. Cervia, E. Assi, F. Simbari, F. Pagni, C. De Palma, et al., Acid sphingomyelinase determines melanoma progression and metastatic behaviour via the microphtalmia-associated transcription factor signalling pathway, Cell Death Differ. 21 (2014) 507–520.
[56] C. Sciorati, T. Touvier, R. Buono, P. Pessina, S. Francois, C. Perrotta, R. Meneveri, et al., Necdin is expressed in cachectic skeletal muscle to protect fibers from tumor-induced wasting, J. Cell Sci. 122 (2009) 1119–1125.
[57] A. Ecker, T. Gonzaga, R.L. Seeger, M.M.D. Santos, J.S. Loreto, A.A. Boligon, D. F. Meinerz, et al., High-sucrose diet induces diabetic-like phenotypes and oxidative stress in Drosophila melanogaster: protective role of Syzygium cumini and Bauhinia forficata, Biomed. Pharm. 89 (2017) 605–616.
[58] D. Cervia, D. Martini, M. Garcia-Gil, G. Di Giuseppe, G. Guella, F. Dini, P. Bagnoli, Cytotoxic effects and apoptotic signalling mechanisms of the sesquiterpenoid euplotin C, a secondary metabolite of the marine ciliate *Euplotes crassus*, in tumour cells, Apoptosis 11 (2006) 829–843.
[59] C. Hetz, The unfolded protein response: controlling cell fate decisions under ER stress and beyond, Nat. Rev. Mol. Cell Biol. 13 (2012) 89–102.
[60] S. Mitra, H.D. Ryoo, The unfolded protein response in metazoan development, J. Cell Sci. 132 (2019) jcs217216.
[61] N. Thakor, B. Janathia, Plumbagin: a potential candidate for future research and development, Curr. Pharmacol. Biotechnol. 23 (2022) 1800–1812.
[62] I. Miguel-Aliaga, H. Jasper, B. Lemaitre, Anatomy and physiology of the digestive tract of drosophila melanogaster, Genetics 210 (2018) 357–396.
[63] S.V. Nair, G. Baranwal, M. Chatterjee, A. Sachu, A.K. Vasudevan, C. Bose, A. Banerji, et al., Antimicrobial activity of plumbagin, a naturally occurring naphthoquinone from Plumbago rosea, against Staphylococcus aureus and Candida albicans, Int. J. Med. Microbiol. 306 (2016) 237–248.
[64] R. Amato, E. Catalani, M. Dal Monte, M. Cammalleri, D. Cervia, G. Casini, Morpho-functional analysis of the early changes induced in retinal ganglion cells by the onset of diabetic retinopathy: the effects of a neuroprotective strategy, Pharmacol. Res. 185 (2022), 106516.
[65] Y. Chen, L. Perusek, A. Maeda, Autophagy in light-induced retinal damage, Exp. Eye Res. 144 (2016) 64–72.
[66] L.S. Frost, C.H. Mitchell, K. Boesze-Battaglia, Autophagy in the eye: implications for ocular cell health, Exp. Eye Res. 124 (2014) 56–66.
[67] P. Boya, L. Esteban-Martinez, A. Serrano-Puebla, R. Gomez-Sintes, B. Villarejo-Zori, Autophagy in the eye: development, degeneration, and aging, Prog. Retin Eye Res. 55 (2016) 206–245.
[68] W. Lin, G. Xu, Autophagy: a role in the apoptosis, survival, inflammation, and development of the retina, Ophthalmic Res. 61 (2019) 65–72.
[69] M. Cammalleri, F. Locri, E. Catalani, L. Filippi, D. Cervia, M. Dal Monte, P. Bagnoli, The beta adrenergic receptor blocker propranolol counteracts retinal dysfunction in a mouse model of oxygen induced retinopathy: restoring the balance between apoptosis and autophagy, Front. Cell Neurosci. 11 (2017) 395.
[70] V. Billes, T. Kovacs, A. Manzeger, P. Lorincz, S. Szincsak, A. Regos, P.I. Kulcsar, et al., Developmentally regulated autophagy is required for eye formation in Drosophila, Autophagy 14 (2018) 1499–1519.
[71] R. Midorikawa, M. Yamamoto-Hino, W. Awano, Y. Hinohara, E. Suzuki, R. Ueda, S. Goto, Autophagy-dependent rhodopsin degradation prevents retinal degeneration in Drosophila, J. Neurosci. 30 (2010) 10703–10719.
[72] Q. Gong, H. Wang, P. Yu, T. Qian, X. Xu, Protective or harmful: the dual roles of autophagy in diabetic retinopathy, Front. Med. 8 (2021), 644121.
[73] M.D. Rosa, G. Distefano, C. Gagliano, D. Rusciano, L. Malaguarnera, Autophagy in diabetic retinopathy, Curr. Neuropharmacol. 14 (2016) 810–825.
[74] R. Amato, E. Catalani, M. Dal Monte, M. Cammalleri, I. Di Renzo, C. Perrotta, D. Cervia, et al., Autophagy-mediated neuroprotection induced by octreotide in an ex vivo model of early diabetic retinopathy, Pharm. Res 128 (2018) 167–178.
[75] Q. Kang, C. Yang, Oxidative stress and diabetic retinopathy: molecular mechanisms, pathogenetic role and therapeutic implications, Redox Biol. 37 (2020), 101799.
[76] L.P. Musselman, J.L. Fink, K. Narzinski, P.V. Ramachandran, S.S. Hathiramani, R. L. Cagan, T.J. Baranski, A high-sugar diet produces obesity and insulin resistance in wild-type Drosophila, Dis. Model Mech. 4 (2011) 842–849.
[77] R. Sawicki, S.P. Singh, A.K. Mondal, H. Benes, P. Zimniak, Cloning, expression and biochemical characterization of one Epsilon-class (GST-3) and ten Delta-class (GST-1) glutathione S-transferases from Drosophila melanogaster, and identification of additional nine members of the Epsilon class, Biochem. J. 370 (2003) 661–669.
[78] V. Ngo, M.L. Duennwald, Nrf2 and oxidative stress: a general overview of mechanisms and implications in human disease, Antioxidants 11 (2022) 2345.
[79] I. Bellezza, I. Giambanco, A. Minelli, R. Donato, Nrf2-Keap1 signaling in oxidative and reductive stress, Biochim. Biophys. Acta Mol. Cell Res. 1865 (2018) 721–733.
[80] A. Pitoniak, D. Bohmann, Mechanisms and functions of Nrf2 signaling in Drosophila, Free Radic. Biol. Med. 88 (2015) 302–313.
[81] O.H. Lee, A.K. Jain, V. Papusha, A.K. Jaiswal, An auto-regulatory loop between stress sensors INrf2 and Nrf2 controls their cellular abundance, J. Biol. Chem. 282 (2007) 36412–36420.
[82] G.P. Sykiotis, D. Bohmann, Keap1/Nrf2 signaling regulates oxidative stress tolerance and lifespan in Drosophila, Dev. Cell 14 (2008) 76–85.
[83] S.M. Boas, K.L. Joyce, R.M. Cowell, The NRF2-dependent transcriptional regulation of antioxidant defense pathways: relevance for cell type-specific vulnerability to neurodegeneration and therapeutic intervention, Antioxid. (Basel) 11 (2021) 8.
[84] I. Moratilla-Rivera, M. Sanchez, J.A. Valdes-Gonzalez, M.P. Gomez-Serranillos, Natural products as modulators of Nrf2 signaling pathway in neuroprotection, Int. J. Mol. Sci. 24 (2023) 3748.
[85] Y. Zhang, Y. Yang, H. Yu, M. Li, L. Hang, X. Xu, Apigenin protects mouse retina against oxidative damage by regulating the Nrf2 pathway and autophagy, Oxid. Med. Cell Longev. (2020) 9420704.
[86] A. Rampin, M. Carrabba, M. Mutoli, C.L. Eman, G. Testa, P. Madeddu, G. Spinetti, Recent advances in KEAP1/NRF2-targeting strategies by phytochemical antioxidants, nanoparticles, and biocompatible scaffolds for the treatment of diabetic cardiovascular complications, Antioxid. Redox Signal 36 (2022) 707–728.
[87] M. Wang, K.J. Sheng, J.C. Fang, H. Zhao, S.M. Lu, Z.Y. Liu, B.T. Chen, Redox signaling in diabetic retinopathy and opportunity for therapeutic intervention through natural products, Eur. J. Med. Chem. 244 (2022), 114829.
[88] N. Robledinos-Anton, R. Fernandez-Gines, G. Manda, A. Cuadrado, Activators and Inhibitors of NRF2: a review of their potential for clinical development, Oxid. Med. Cell Longev. (2019) 9372182.
[89] P.D. O'Brien, L.M. Hinder, S.A. Sakowski, E.L. Feldman, ER stress in diabetic peripheral neuropathy: a new therapeutic target, Antioxid. Redox Signal 21 (2014) 621–633.
[90] P.S. Lange, J.C. Chavez, J.T. Pinto, G. Coppola, C.W. Sun, T.M. Townes, D. H. Geschwind, et al., ATF4 is an oxidative stress-inducible, prodeath transcription factor in neurons in vitro and in vivo, J. Exp. Med. 205 (2008) 1227–1242.
[91] P.M. Pitale, O. Gorbatyuk, M. Gorbatyuk, Neurodegeneration: keeping ATF4 on a tight leash, Front. Cell Neurosci. 11 (2017) 410.
[92] S. Zielke, S. Kardo, L. Zein, M. Mari, A. Covarrubias-Pinto, M.N. Kinzler, N. Meyer, et al., ATF4 links ER stress with reticulophagy in glioblastoma cells, Autophagy 17 (2021) 2432–2448.
[93] K. Kang, H.D. Ryoo, J.E. Park, J.H. Yoon, M.J. Kang, A drosophila reporter for the translational activation of ATF4 marks stressed cells during development, PLoS One 10 (2015), e0126795.
[94] H.D. Ryoo, Drosophila as a model for unfolded protein response research, BMB Rep. 48 (2015) 445–453.
[95] E. Catalani, S. Zecchini, M. Giovarelli, A. Cherubini, S. Del Quondam, K. Brunetti, F. Silvestri, et al., RACK1 is evolutionary conserved in satellite stem cell activation and adult skeletal muscle regeneration, Cell Death Discov. 8 (2022) 459.
[96] D. Vasudevan, S.D. Neuman, A. Yang, L. Lough, B. Brown, A. Bashirullah, T. Cardozo, et al., Translational induction of ATF4 during integrated stress response requires noncanonical initiation factors eIF2D and DENR, Nat. Commun. 11 (2020) 4677.
[97] F. Tian, Y. Cheng, S. Zhou, Q. Wang, A. Monavarfeshani, K. Gao, W. Jiang, et al., Core transcription programs controlling injury-induced neurodegeneration of retinal ganglion cells, Neuron 110 (2022) 2607–2624, e2608.
[98] M. Wang, R.J. Kaufman, Protein misfolding in the endoplasmic reticulum as a conduit to human disease, Nature 529 (2016) 326–335.
[99] P. Walter, D. Ron, The unfolded protein response: from stress pathway to homeostatic regulation, Science 334 (2011) 1081–1086.